ADVANCED ENERGY MATERIALS

Supporting Information

for *Adv. Energy Mater.,* DOI: 10.1002/aenm.201600379

A Stabilized, Intrinsically Safe, 10% Efficient, Solar-Driven Water-Splitting Cell Incorporating Earth-Abundant Electrocatalysts with Steady-State pH Gradients and Product Separation Enabled by a Bipolar Membrane

Ke Sun, Rui Liu, Yikai Chen, Erik Verlage, Nathan S. Lewis, and Chengxiang Xiang**

Supporting Information

A Stabilized, Intrinsically Safe, 10% Efficient, Solar-Driven Water-Splitting Cell Incorporating Earth-Abundant Electrocatalysts with Steady-State pH Gradients and Product Separation Enabled by a Bipolar Membrane

Ke Sun,[1,2] Rui Liu,[1] Yikai Chen[1], Erik Verlage,[1,3] Nathan S. Lewis,[1,2,4,5] Chengxiang Xiang*[1]*

1. Joint Center for Artificial Photosynthesis, California Institute of Technology, Pasadena CA 91125, USA

2. *Division of Chemistry and Chemical Engineering, 210 Noyes Laboratory, 127-72, California Institute of Technology, Pasadena, CA 91125, USA*

3. *Department of Applied Physics and Materials Science, California Institute of Technology, Pasadena, CA 91125, USA*

4. Beckman Institute and Molecular Materials Research Center, California Institute of Technology, Pasadena, CA 91125, USA

5. Kavli Nanoscience Institute, California Institute of Technology, Pasadena, CA 91125, USA

*To whom correspondence should be addressed: nslewis@caltech.edu and cxx@caltech.edu

Chemicals and materials

All materials were used as received, except where otherwise noted. Deionized H_2O with a resistivity of >18.2 MΩ-cm was obtained from a Millipore deionized water system. A 0.5 M potassium borate solution was prepared using a 0.5 M KOH(aq) solution made from potassium hydroxide pellets (KOH, Macron Chemicals, ACS 88%) and 1 M boric acid (H_3BO_3, Sigma-Aldrich, BioReagent ≥99.5%) aqueous solution, for all electrochemical measurements. Ultrapure sulfuric acid (H_2SO_4, J. T. Baker, ACS reagent, 95%-98%). The Ag-based conductive epoxy was obtained from SPI supplies. The bipolar membrane (fumasep® FBM) was purchased from FuMA-Tech GmbH (St. Ingbert, Germany) and was stored in 1.0 M NaCl(aq) at room temperature. Bipolar membranes were cut into 3×3 cm pieces and were thoroughly rinsed with deionized H_2O water before use. Nafion® PFSA 117 membrane (Chemours) with a thickness of 183 µm was purchased from Dupont. Membrane was soaked in DI water for at least 4 hours and rinsed with DI water before use.

Growth of III-V tandem photoabsorbers

The tandem junction device was grown commercially (Sumika Electronic Materials, Inc.) according to specifications determined by 1-D numerical simulation using Helmholtz-Zentrum Berlin's AFORS-HET software. Planar III-V layers were grown epitaxially by metal-organic chemical vapor deposition (MOCVD) on an n^+-GaAs wafer that had a (100)-oriented polished surface (Si-doped, acceptor concentration of 1×10^{19} cm^{-3}, 6" diameter). Detailed information on the cell stack, including the thickness and the dopants for the III-V layers, has been provided previously.[1]

Atomic layer deposition of the protective TiO_2 layer

TiO_2 films were deposited on the exposed p^+-GaAs epilayer at 150 °C using an Ultratech Fiji 200 plasma atomic-layer deposition (ALD) system. Prior to ALD, the

epitaxial surface was immersed for 30 s in 1.0 M KOH(aq) (aqueous solution of potassium hydroxide pellets, semiconductor grade, 99.99% trace metals basis, Sigma-Aldrich), rinsed with copious amounts of deionized H_2O, dried using a stream of N_2(g), and loaded immediately thereafter into the ALD chamber. Each ALD cycle consisted of a 0.06 s pulse of H_2O (>18.2 MΩ-cm resistivity, Millipore), followed by a 0.25 s pulse of tetrakis(dimethylamido)titanium (TDMAT, Sigma-Aldrich, 99.999%, used as received). A 15 s purge under a constant 0.13 L min^{-1} flow of research-grade Ar(g) was performed between each precursor pulse. The base pressure during the TiO_2 growth was maintained at ~0.1 Torr. ALD-TiO_2 films with thicknesses of 62.5 nm were used to protect III-V surfaces, as well as to ensure proper current matching and thus a maximized photocurrent density under 1 Sun illumination.

Deposition of electrocatalysts and ohmic contacts

Ohmic contact to the n^+-GaAs wafer was formed using a Ge-Au eutectic (20 nm Ge/ 30 nm Au/ 15 nm Ni/ 100 nm Au) deposited by radio-frequency (RF) sputtering. The contact layers were annealed under N_2(g) at 400 °C for 30 s using rapid thermal annealing (RTA) with a ramp-up rate of 40 °C s^{-1}. For all photoanode surfaces, an optically transparent (nominally 2 nm thick) Ni film was deposited on TiO_2 using RF sputtering (AJA international) at 130 W with a constant deposition rate of ~0.1 Å s^{-1} at a constant working pressure of 5 mTorr maintained by a Ar flow rate of 10 sccm.

ALD-deposited amorphous TiO_2 coatings have been used on various single crystalline substrates, including Si, IIIV and II-VI compound semiconductors previously which showed excellent ohmic behavior due to similar growth chemistry.[1, 2] Degenerately doped Si substrates with an acceptor (hole) concentration>10^{19} cm^{-3} p^+-Si were used in this study as the dark electrode control sample, to be consistent with the actual sample which had a window layer consisting of a 30-nm p^+-$In_{0.48}Al_{0.57}P$ and a 7-nm thick p^+-GaAs with acceptor concentrations >10^{19} cm^{-3}. Atomically-flat single

crystalline substrates was also used to ensure the catalyst loading especially in terms of morphology controlled by surface energy is comparable.

Counter electrodes were either a Pt mesh or a Ti mesh. The Ti mesh electrodes were coated by electrodeposition of CoP, as described previously.[3] To minimize leaching of Co into the catholyte, the CoP counter electrode was electrochemically conditioned in a separate home-made cell with 1.0 M H_2SO_4(aq) in the dark using a three-electrode configuration, prior to transferring the cathode to the water-splitting cell. This electrochemical conditioning was conducted using cyclic voltammetry with a potential window of -0.15~0.05 V vs. RHE at a scan rate of 10 mV s^{-1} for at least 20 cycles, to remove excess Co metal in the Co phosphide film.

Preparation of electrodes for 3-electrode and 2-electrode electrochemical measurements

For use in photoelectrochemical cells, the ohmically contacted tandem-junction wafers were cleaved into samples 0.5~1.5 cm^2 in area. High-purity Ag paint (SPI supplies) was then used to mechanically attach the ohmic contact to a coiled, tin-plated Cu wire (McMaster-Carr) that was then threaded through a glass tube (Corning Incorporation, Pyrex tubing, 7740 glass). The sample was encapsulated and sealed to the glass tube using grey epoxy (Hysol 9460F). The epoxy was allowed to dry under ambient conditions for > 12 h. A high-resolution optical scanner (Epson perfection V370 with a resolution of 2400 dpi) was used to image the exposed surface area of each electrode, and the geometric areas were determined by analyzing the images using ImageJ software. All of the electrodes used were 0.1-0.2 cm^2 and ~1 cm^2 in area for 3-electrode and 2-electrode electrochemical measurements, respectively.

Photoelectrochemical and electrochemical measurement

A saturated calomel electrode (SCE, CH Instruments) was used as a reference electrode for all three-electrode photoelectrochemical measurements. The pH of the 0.5 M KBi(aq) solution was 9.3, as measured using a VWR SympHony SB70P Digital, Bench-model pH Meter. The SCE reference electrodes were calibrated in 0.5 M KBi(aq) using a reversible hydrogen electrode (RHE) fabricated from a homemade Pt disc in contact with a continuous purge of 1 atm of H_2(g). The RHE potential was -0.796 V vs. SCE. The equilibrium potential for water oxidation in 0.5 M KBi(aq) was therefore calculated to be 0.434 V vs. SCE.

3-electrode measurements:

A custom electrochemical cell with a flat glass (Pyrex) bottom was used for all of the 3-electrode (photo)electrochemical measurements (Figure S1a). The electrolyte was vigorously agitated with a magnetic stir bar driven by a model-train motor (Pittman) with a Railpower 1370 speed controller (Model Rectifier Corporation). The data presented for electrochemical measurements in aqueous solutions do not include compensation for the series resistance of the solution. A Xe arc lamp (Newport 67005 and 69911) equipped with an IR filter (Newport 61945) and with an AM 1.5 filter (Newport 81094 and 71260) was used as the light source for *J-E* measurements and for the spectral response measurements. The illumination intensity at the position of the working electrode in the electrochemical cell was determined by placing a calibrated Si photodiode (FDS100-Cal, Thor Labs) into the cell at the same position occupied by the exposed area of the photoelectrode. To illuminate bottom-facing photoelectrodes, a quartz diffuser (Newport 15Diff-Vis) together with a broadband reflection mirror (Newport dielectric mirror, 10Q20PR-HR) was used to direct the uniform light beam from the horizontal to the

vertical direction. ELH-type (Sylvania/Osram) and ENH-type (EIKO) tungsten-halogen lamps, which were mounted in a home-made housing and were powered by a transformer (Staco Energy Products Co.), were used for long-term photoelectrochemical stability measurements.

Cyclic voltammetric and chronoamperometric data were obtained using a Biologic SP-200 potentiostat (Bio-Logic Science Instrument). The cyclic voltammetric data were recorded at a scan rate of 40 mV s^{-1} with a scan range that varied depending on the photovoltage and the open-circuit potential of the sample. Samples sizes in the 3-electrode measurement were typically ~0.2 cm^2.

2-electrode BMP-containing cell measurements:

Two custom-made three-necked cells, with a flat quartz window for side-facing illumination and side connectors, were used in the 2-electrode BPM electrochemical measurements (Figure S1b). In addition to the stirring described above, a peristaltic pumping system (Simply Pumps PM300F) with a minimal flow rate of ~ 500 mL min^{-1} controlled by a tunable power supply was used to facilitate the removal of bubbles from the sample surface and to minimize the dissolution of the Ni catalysts at near-neutral pH. Curved glass tubing was connected to the pump through polyimide tubing, and was placed close to the sample surfaces for efficient circulation. The resistance losses in the two-compartment configuration with the bipolar membrane were obtained from current-interruption measurements at a constant current of 10 mA using a Ni mesh in the anolyte chamber and a Pt mesh in the catholyte chamber. For photoelectrochemical experiments, the illumination intensity from a class AAA solar simulator (ABET Technologies, Inc.) was first measured based on an NREL-calibrated Si photovoltaic reference cell. The intensity in the solution-containing cell was then calibrated by placing a Si photodiode (Thor Labs) in the custom-made three neck beaker with flat quartz windows at the same location occupied by the exposed area of the photoelectrode. The Si photodiode had been

previously calibrated by measurement of the short-circuit current density under AM 1.5 simulated sunlight at 100 mW cm^{-2} (1-Sun) with the irradiance provided by a Xe arc lamp with an AM 1.5 filter.

Cyclic voltammetric and chronoamperometric data were obtained using a Biologic SP-200 potentiostat (Bio-Logic Science Instrument). The 2-electrode voltammetric data were recorded at a scan rate of 40 mV s^{-1} by connecting RE and CE on the CE mesh, and the scan range was varied depending on the photovoltage and the open-circuit potential of the sample. The voltage range was also confined to be more positive than the onset of photoanodic current, to ensure a constant direction of ionic current flow in the membrane. ~Samples ~1 cm^2 in area were used for the 2-electrode measurements.

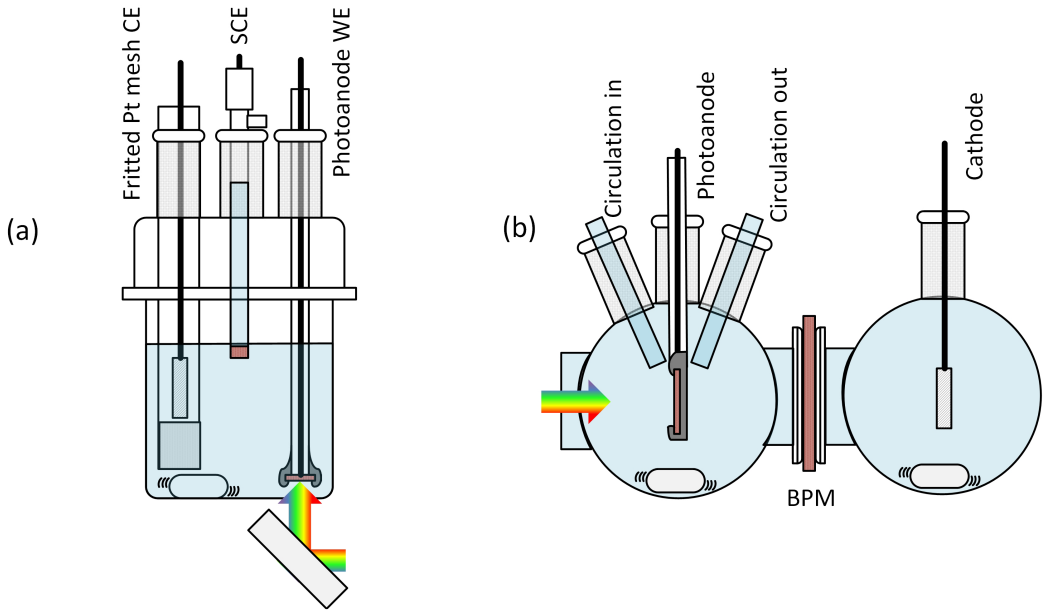

Figure S1. Schematic showing the measurement setup for 3-electrode (a) and 2-electrode (b) electrochemical measurements.

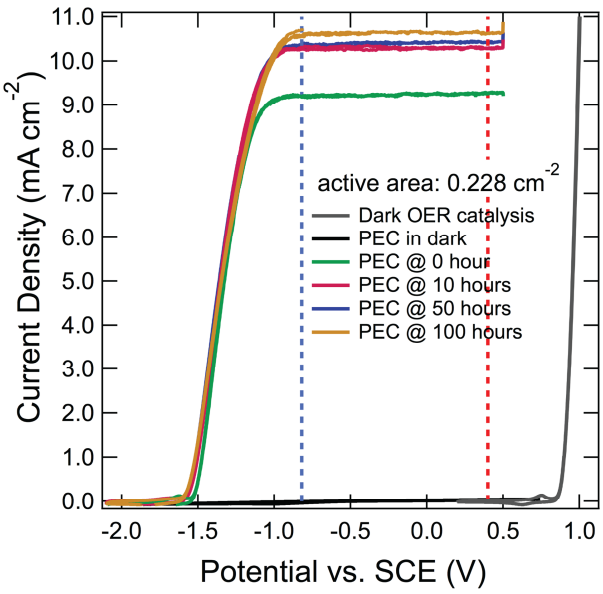

Figure S2. Cyclic voltammetry of GaAs/InGaP/TiO_2/Ni photoanode in contact with a 0.5 M potassium borate buffer solution (KBi) at pH=9.3 in the dark (black) and under 1 sun of simulated solar illumination (red) at 0, 10, 50 and 100 hours during the stability test. The photocurrent density measurements during the stability test was shown in Figure 1b. The equilibrium potentials at pH=9.3 for the oxygen-evolution reaction (OER) and the hydrogen-evolution reaction (HER) are indicated by the dotted lines.

Load-line analysis:

The details of a load-line analysis can be found in references 3,4. Briefly, the photoelectrode performance is treated in a simplified equivalent circuit approach as a photovoltaic cell connected in series electrically with a dark electrolysis cell. The photovoltaic parameters including the open-circuit voltage (V_{oc}), the short-circuit current density (J_{sc}), the fill factor (FF) and the energy-conversion efficiency (η) are then

evaluated by subtracting the dark electrolysis *J-E* data obtained using a p^+-Si|TiO_2|Ni dark electrode from the *J-E* data exhibited by the illuminated photoelectrode under evaluation.

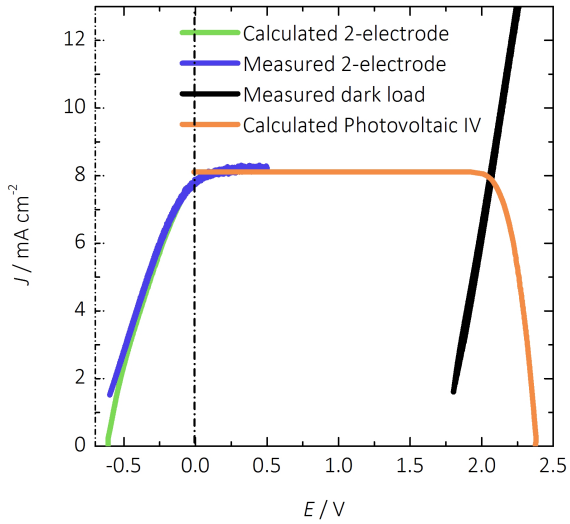

Figure S3. Measured and calculated 2-electrode *J-E* behavior. Orange curve: calculated solid-state photovoltaic *I-V* behavior from 3-electrode data shown in Figure 1a. Black curve: measured 2-electrode *J-V* behavior using a p^+-Si|TiO_2|Ni anode and a Ti/CoP cathode in the same BMP configuration. Blue curve: measured 2-electrode *J-V* behavior using a GaAs/InGaP/TiO_2/Ni photoanode under simulated AM1.5 1-Sun illumination and a Pt mesh cathode in a BMP configuration. Green curve: calculated 2-electrode *J-V* behavior obtained by subtracting the dark curve from the orange curve.

Calculation of Solar-to-hydrogen Conversion Efficiency (η_{STH}):

The Solar-to-hydrogen conversion efficiency, $\eta_{STH,}$ using equation:

$$\eta_{\mathrm{STH}} = {1.23\ \mathrm{V} \times J_{\mathrm{electrode}}\ \mathrm{mA \cdot cm^{-2}}}/{100\ \mathrm{mW \cdot cm^{-2}}} \qquad \text{(Eq.s1)}$$

No chemical bias exists in the system, because at steady-state, the only reagent consumed is $H_2O(l)$; no change results during operation in the composition of the anolyte, catholyte, electrodes, or membrane in the system, and the chemical outputs are 1 atm of $H_2(g)$ and $O_2(g)$ under standard conditions.

Four-point measurement system for the bipolar membrane

Figure S4 illustrates the experimental apparatus for the membrane voltage measurements. The diameters of the O-rings used in the apparatus were 0.5" and 0.75", respectively, and hence the resulting membrane area was ~2.3 times larger than the electrode area. A compact flow cell was designed and constructed as the chassis for measurement of the electrical potential drop across the membrane during steady-state operation. Two Ag/AgCl reference electrodes were placed ~ 2 mm from the bipolar membrane, and two Pt electrodes were used as the source and the drain electrodes during the measurements. The current between the two Pt electrodes was swept, and the resulting potential difference between the two reference electrodes was recorded. A peristaltic pumping system (with a flow rate of ~ 10 mL min^{-1}) was used to facilitate removal of bubbles from the Pt electrode surfaces and to minimize the pH gradients at the electrode surface during steady-state operation.

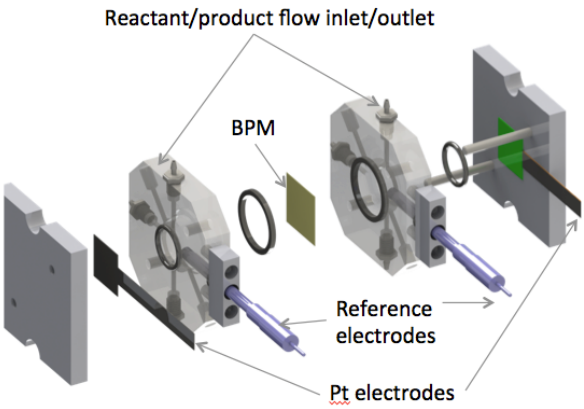

Figure S4: A schematic illustration of the four-point setup for measuring the potential drops across the bipolar membrane.

Faradaic efficiency measurements for O_2 generation:

Measurements of the Faradaic efficiency based on collection of the evolved O_2(g) were conducted using a custom eudiometer apparatus that consisted of an inverted burette that was connected to a three-necked electrochemical cell. The cell was configured using the 3-electrode electrochemical measurement apparatus described above, with the working electrode of surface area of 1-1.06 cm^{-2} placed inside the inverted burette. Three replicates were measured directly without prior activation of the catalyst in 0.5 M KBi(aq). A bias sufficient to produce a constant current of 5 mA was then applied using a potentiostat configured to act as a power supply. The bias was automatically adjusted to maintain a constant current throughout the measurement, with illumination of the photoanode provided by a halogen lamp through the burette glass wall. The expected volume of O_2(ml) generated was calculated based on the charge passed (C in coulombs) using the equation:

$$O_2\ volume(ml) = \frac{1000 \cdot T \cdot \rho \cdot C}{4 \cdot F \cdot M_w} \qquad \text{(Eq.s2)}$$

where T is temperature (296.45 K), ρ is the O_2 density at atmospheric pressure (1.43 g cm^{-3}), C is the total charge passed (C), F is Faraday's constant (9.65×10^4 C mol^{-1}), and M_w is the molecular weight of O_2 (15.99 g mol^{-1}). The Faradaic efficiency was calculated as the ratio of the measured to the expected O_2 volume.

ICP-MS ion crossover measurements

Ion concentrations in the analyte and catholyte in a 2-electrode BPM configuration at different time during the stability test were determined by Inductively Coupled Plasma – Mass Spectrometry using an Agilent 8800 spectrometer. The sample-introduction system consisted of a MicroMist nebulizer with a Scott-type spray chamber. A fixed-injector quartz torch was used with a guard electrode and the plasma was operated at 1500 W. In addition to single-quad (MS) mode with no gas, elements were determined by MS-MS modes where different collision or reactive gasses were present in the gas cell located between the quadrupoles. These modes were no-gas, helium, hydrogen and oxygen. Phosphorus, sulfur, titanium, arsenic and yttrium in particular were determined using oxygen mode with a mass shift of +16 m/z (+O) from Q1 to Q2. External standards were used to quantify the analytes determined.

Product-gas crossover measurements

The gas permeability of fully hydrated membranes was measured using the experimental arrangement shown in Figure S5. The membranes were sandwiched between two plastic plates that had dimensions of 48 × 48 × 5 mm. On the side away

from the membrane, each plate had an inlet and an outlet port that led to/from a circular chamber with a diameter of 17 mm. The membrane-facing side of the circular chamber had a circular opening, 7 mm in diameter, which contacted the membrane and served as the membrane contact area for the gas-permeation measurement. On one side of the "sandwich", the H_2 or O_2 stream was passed through a gas-washing bottle that was filled with water, to humidify the gas before it entered into the cell. Once in the cell, the gas would either diffuse across the membrane or exit the cell through the outlet into a flask of water open to the atmosphere. In this way, any pressure rise in the cell could be minimized. On the right side, deionized water was circulated through the cell and a Unisense Hydrogen Sensor H_2-100 or O_2 sensor was used to measure the concentration of H_2 or O_2 in the circulating water. The gas flow rate was low (10 sccm), to minimize any gas transport driven by pressure differentials. The measurements of H_2 and O_2 permeability were repeated three times for each sample; reported values are the average of these measurements.

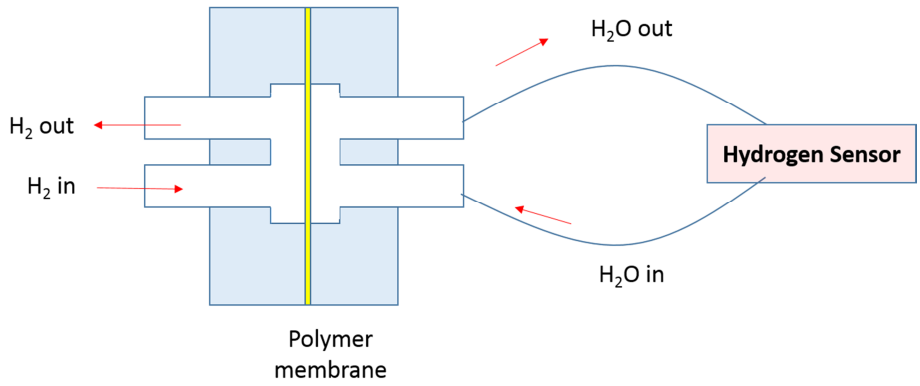

Figure S5: A schematic illustration of the experimental setup for the measurement of product-gas crossover in Nafion 117 membrane and in fumasep® FBM bipolar membranes (not drawn to scale).

Table S1: Product gas permeability measurements in the bipolar membrane and in Nafion.

	H_2 Diffusion Coefficient, $10^6 D$ ($cm^2\ s^{-1}$)	H_2 Solubility $10^6 c^0$ (mol cm^{-3})	H_2 Permeability $10^{12}\ Dc^0$ (mol $cm^{-1}\ s^{-1}$)	O_2 Diffusion Coefficient, $10^6 D$ ($cm^2\ s^{-1}$)	O_2 Solubility $10^6 c^0$ (mol cm^{-3})	O_2 Permeability $10^{12}\ Dc^0$ (mol $cm^{-1}\ s^{-1}$)
Nafion 117	7.6	0.5	3.8	0.40	5.0	2.0
FUMA SEP® FBM	3.6	0.3	1.1	0.18	2.5	0.45

Substrate stability: SEM and EDS

Visible defects were observed using scanning-electron microscopy (SEM) on at least 3 GaAs/InGaP/TiO_2/Ni photoanodes with areas of ~1 cm^2 after 100 h of continuous operation in the BMP configuration. However, not all visible defects or pin-hole like features (highlighted by red circles in Figure S6) led to catastrophic substrate etching. In most regions of the electrodes, SEM images of the photoelectrodes after the stability measurements (Figure S6) did not exhibit any substantial changes as compared to fresh prepared photoelectrodes. Energy-dispersive spectroscopy (EDS) was conducted on these defect-like features and revealed the existence of the catalyst, protective layer and top junction (right panel of the EDS spectrum in Figure S6). However, spectra at the large hole resulting from a catastrophic etching of the substrate only showed signals from the GaAs substrates, suggesting the complete removal of the epilayer (4 µm), the protective coating, as well as the catalyst (left panel of the EDS spectrum in Figure S6).

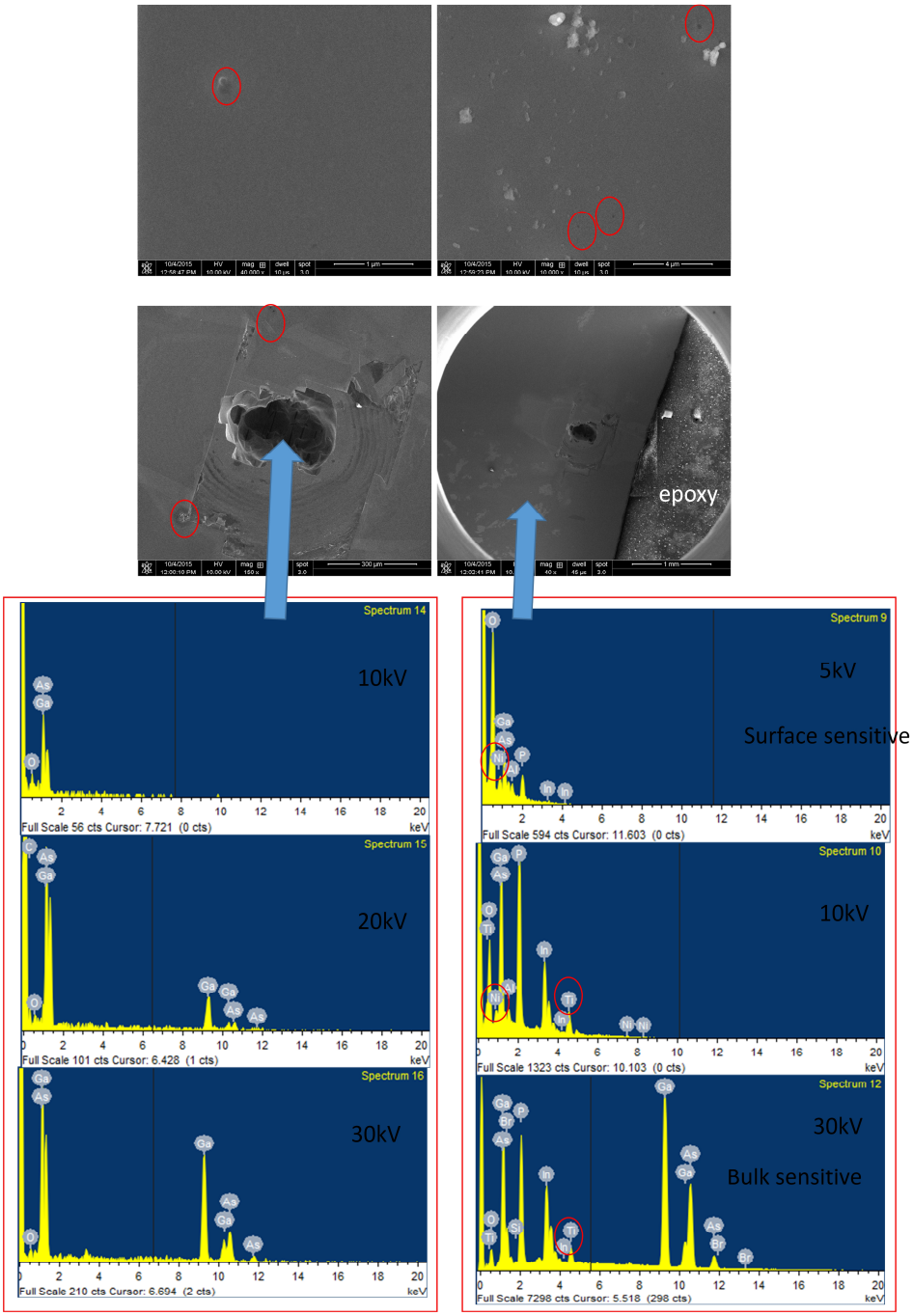

Figure S6. Representative SEM images on a GaAs/InGaP/TiO_2/Ni photoanode after stability test in a BMP configuration showing substrate etching and defect-like features on the surface. EDS spectra at the surface with different incident electron energies for different excitation volumes to probe the substrate at different depth.

Charge density needed to dissolve the tandem junction epilayer:

Assuming that the average current density was 8 mA cm^{-2} during the 100 h continuous operation, the charge passed per cm^2 is:

$$8 \times 10^{-3} \times 100 \times 60 \times 60\ C\ cm^{-2} = 2880\ C\ cm^{-2} \quad \text{(Eq.s3)}$$

The thickness of epilayer is 4 μm, and the average mass density of the epilayer is 4.8 g cm^{-3}. Assuming that the epilayer was oxidized to form GaO_2 and AsO_2, the charge density passed would be:

$$\frac{0.004 \times 10^{-1} \times 1 \times 4.8}{128.7} \times 4 \times 96500\ \text{cm}^{-2} = 57\ \text{C cm}^{-2} \quad \text{(Eq.s4)}$$

The ratio of the total charge passed to the charge required to dissolve Si wafer is thus:

$$\frac{57}{2880} \approx 0.02 \quad \text{(Eq.s5)}$$

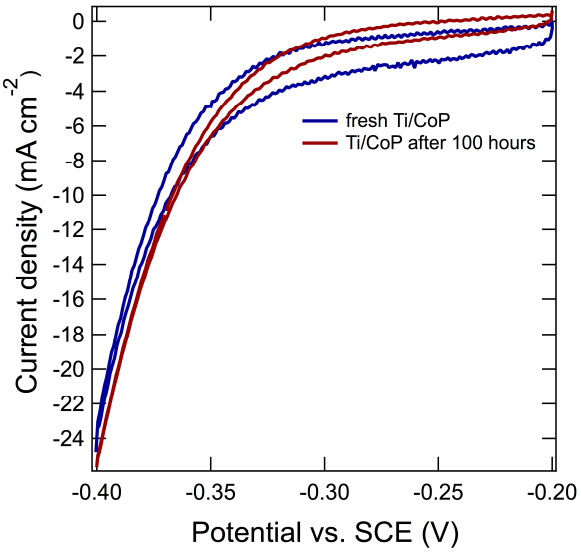

Figure S7. Cyclic voltammetry of Ti/CoP catalysts in 1.0 M H_2SO_4 (aq) before (blue) and after (red) the 100-hour stability test.

Table S2. Comparison of selected properties of solar-driven water splitting cells using a bipolar membrane operating at 1.0 M H_2SO_4 (aq)/0.5M KBi(aq) vs using an AEM operating in 1.0 M KOH(aq)

Components	**Voltage loss at $J_{electrode}$=10 mA cm^{-2}**	
	1.0 M KOH	1.0 M H_2SO_4/0.5M K-Bi (This work)
Membrane	~ 50 – 100 mV (AEM)	~ $V_{membrane,\ loss}$ ~ 400 - 500 mV (AEM/CEM) at $J_{membrane}$ =4.36 mA cm^{-2}
Transparent OER overpotential	~340 mV/NiO_x[4]	~660 mV/NiO_x
Dark HER overpotential	~100 mV/NiMo[5]	~100 mV/CoP
Total voltage loss	>490 mV	>1200 mV

Numerical modeling of the bipolar membrane/electrolyte interface

Model setup

Governing Equations

The Poisson equations (Eq.s6 and Eq.s7) and the Nernst-Planck equation (Eq. s8) were coupled together in a commercially available software package, COMSOL to model the electrical potential and species transport in the bipolar membrane:

$$E = -\nabla V \quad \text{(Eq.s6)}$$

$$\nabla \cdot (\varepsilon_0 \varepsilon_r E) = \rho_V \quad \text{(Eq.s7)}$$

$$\nabla \cdot (-D_i \nabla c_i - z_i u_{m,i} F c_i \nabla V) = \mathrm{R}_i \quad \text{(Eq.s8)}$$

where E is the electric field, V is the scalar electric potential field, ε_0 and ε_r are the vacuum permittivity with values of 8.854×10^{-12} F m^{-1} and the relative permittivity of the material in each calculated domain, respectively, ρ_V is the space-charge density, D_i is the diffusion coefficient for the species i in the specified domain (Table s3), c_i and z_i are the concentration and charge number of the species i, respectively, and $u_{m,i}$ is the mobility defined by the Nernst-Einstein relation (Eq. s9):

$$u_{m,i} = \frac{D_i}{RT} \quad \text{(Eq.s9)}$$

where R is the gas constant, T is the absolute temperature, F represents Faraday's constant, and R_i accounts for the chemical reaction rate for the species i.

In the electrolyte, buffer and water equilibria were also included in the simulation:

$$H_3BO_3 \underset{k_{1b}}{\overset{k_{1f}}{\rightleftharpoons}} H_2BO_2^- + H^+ \quad \text{(Eq.s10)}$$

and

$$H_2O \underset{k_{2b}}{\overset{k_{2f}}{\rightleftharpoons}} H^+ + OH^- \text{ . (Eq.s11)}$$

where k_f and k_b are the corresponding forward and reverse rate constants for each reaction, respectively (Table s4).

Initial conditions and Boundary Conditions

The concentration of the fixed positive charge in the AEM and the concentration of the fixed negative charge in the CEM were both set to 1.0 M. The concentration of the mobile species, the proton in CEM and the hydroxide in AEM, was set to 1.0 M. The boundary electric potential was set to 0 (=59 mV × $pH_{0,CEM}$) for the CEM and 826 mV (=59 mV × $pH_{0,AEM}$) for the AEM. In the borate electrolyte region, the hydrodynamic boundary layer thickness was set to 500 μm and at the hydrodynamic boundary layer, the concentrations of all the solution species were fixed. Continuity was assumed at the AEM/CEM interface and the membrane/electrolyte interface.

The pH, electrochemical and fixed charge-density profiles in the bipolar membrane system

Figure S8 shows the pH, electric potential, and space-charge density profiles as a function of position for the bipolar membrane system. For a bipolar membrane composed of 100-micron-thick CEM and AEM sides, all transitions of pH, electric potential and space-charge density occur within 10 nm of the interface between the CEM and AEM sides. The pH value increases from 0 in the CEM to 14 in the AEM, while the

electric potential increases from 0 to 826 mV. The space-charge density decreased from 0 to -9.64×10^7 C m^{-3} on the CEM side and decreased from 9.64×10^7 C m^{-3} to 0 on the AEM side that was responsible for the electric potential change at the interface.

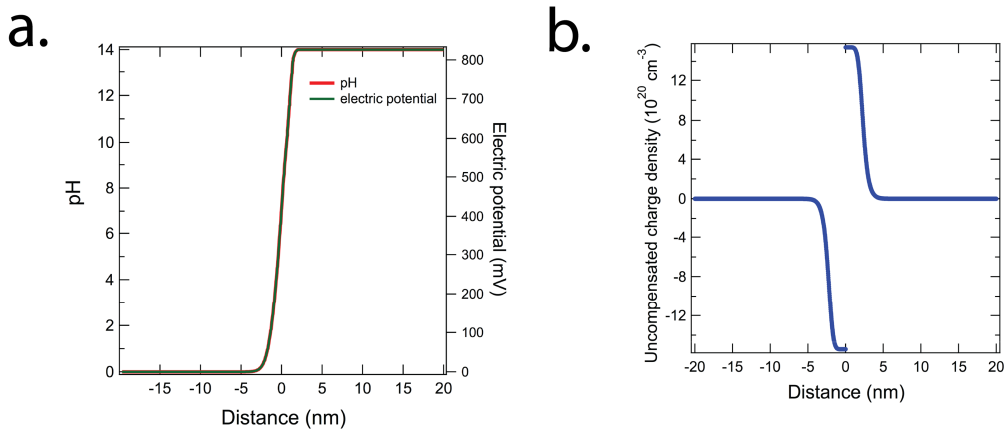

Fig.S8 a) Simulated pH profile and electric potential profile across the transition region of the bipolar membrane, b) simulated uncompensated charge density across the transition region of the bipolar membrane.

Table S3. Diffusion coefficients for the species included in the simulation.

H^+ in membrane, $D_{H^+,m}$	0.5x10^{-6} cm^2 s^{-1}
OH^- in membrane, $D_{OH^-,m}$	0.28x10^{-6} cm^2 s^{-1}
H^+ in the solution, $D_{H^+,s}$	9.31x10^{-5} cm^2 s^{-1}
OH^- in the solution, $D_{OH^-,s}$	5.26x10^{-5} cm^2 s^{-1}
$H_2BO_2^-$ in the solution, $D_{H_2BO_3^-,s}$	0.879x10^{-5} cm^2 s^{-1}
H_3BO_3 in the solution, $D_{H_3BO_3,s}$	1.325x10^{-5} cm^2 s^{-1}
K^+ in the solution, $D_{K^+,s}$	1.96x10^{-5} cm^2 s^{-1}

Table S4. The forward and the backward rate constants used in the simulation.

$H_3BO_3 \underset{k_{1b}}{\overset{k_{1f}}{\rightleftharpoons}} H_2BO_2^- + H^+$	k_{1f}=1x10^7 s^{-1} k_{1b} =1.74x10^{16} M^{-1} s^{-1}
$H_2O \underset{k_{2b}}{\overset{k_{2f}}{\rightleftharpoons}} H^+ + OH^-$	K_{2f} =1x10^8 s^{-1} K_{2b} =1x10^{19} M^{-1} s^{-1}

References:

[1] E. Verlage, S. Hu, R. Liu, R. J. R. Jones, K. Sun, C. Xiang, N. S. Lewis, H. A. Atwater, Energy Environ. Sci. 2015, **8**, 3166.

[2] S. Hu, M. R. Shaner, J. A. Beardslee, M. Lichterman, B. S. Brunschwig, N. S. Lewis, Science 2014, **344**, 1005; M. F. Lichterman, K. Sun, S. Hu, X. Zhou, M. T. McDowell, M. R. Shaner, M. H. Richter, E. J. Crumlin, A. I. Carim, F. H. Saadi, B. S. Brunschwig, N. S. Lewis, Catal. Today 2016, **262**, 11; M. F. Lichterman, A. I. Carim, M. T. McDowell, S. Hu, H. B. Gray, B. S. Brunschwig, N. S. Lewis, Energy Environ. Sci. 2014, **7**, 3334.

[3] F. H. Saadi, A. I. Carim, E. Verlage, J. C. Hemminger, N. S. Lewis, M. P. Soriaga, J. Phys. Chem. C 2014, **118**, 29294.

[4] K. Sun, F. H. Saadi, M. F. Lichterman, W. G. Hale, H.-P. Wang, X. Zhou, N. T. Plymale, S. T. Omelchenko, J.-H. He, K. M. Papadantonakis, B. S. Brunschwig, N. S. Lewis, Proc. Natl. Acad. Sci. USA 2015, **112**, 3612.

[5] J. R. McKone, B. F. Sadtler, C. A. Werlang, N. S. Lewis, H. B. Gray, ACS Catalysis 2013, **3**, 166.